A LETTERS JOURNAL EXPLORING THE FRONTIERS OF PHYSICS

Società Italiana di Fisica

edp sciences IOP Institute of Physics

LETTER

Polarization-multiplexed broadband hologram on all-dielectric metasurface

To cite this article: Z. F. Li *et al* 2018 *EPL* **124** 14003

A LETTERS JOURNAL EXPLORING THE FRONTIERS OF PHYSICS

October 2018

EPL, **124** (2018) 14003
www.epljournal.org
doi: 10.1209/0295-5075/124/14003

Polarization-multiplexed broadband hologram on all-dielectric metasurface

Z. F. Li[1], P. W. Qiao[1], G. Y. Dong[1(a)], Y. S. Shi[1(b)], K. Bi[2(c)], X. L. Yang[3] and X. F. Meng[3]

[1] *College of Opto-Electronic Technology, University of Chinese Academy of Sciences - Beijing 100049, China*
[2] *State Key Laboratory of Information Photonics and Optical Communications & School of Science, Beijing University of Posts and Telecommunications - Beijing 100876, China*
[3] *Department of Optics, Shandong University - Jinan 250100, China*

received 28 July 2018; accepted in final form 27 September 2018
published online 5 November 2018

PACS 42.70.Ln – Holographic recording materials; optical storage media
PACS 42.25.Ja – Polarization
PACS 81.05.Xj – Metamaterials for chiral, bianisotropic and other complex media

Abstract – Metasurface is emerging as an important platform to design various functional devices due to the superior capability in controlling amplitude, phase and polarization of light through its ultrathin engineering interface. A polarized-selective hologram of all-dielectric metasurface is proposed to reconstruct multiplexed holographic images on different linear polarization status. Unlike early metasurfaces composed of plasmonic resonators with great ohmic loss at visible spectrum, the designed metasurface made of silicon nanoblocks supports a broader spectral response over the bandwidth from 600 to 760 nm with high diffraction efficiency and low crosstalk between different polarization states. Both simulation and experiment have demonstrated the feasibility and adjustability of the polarization-multiplexed metasurface hologram. We believe it will have significant technological potential in the design of optical functional devices.

Introduction. – The polarization-multiplexed holograms are sensitive to the polarization of incident light and can reconstruct different holographic images by separating the readout light through its polarization status, leading various applications in optical information fields, such as optical storage [1], encryption [2], multistage optical switching [3] and optical interconnection network [4]. So far, various methods to realize polarization-dependent holograms have been proposed and demonstrated. Traditional polarization-selective holograms are typically built from either a naturally birefringent crystals with surface-relief profile [5,6] or form-birefringent materials with sub-wavelength microstructures [7,8], which provide effective methods for processing two independent orthogonal polarizations. However, most of them suffered from narrow operating bandwidth so that the amplitudes and phases of modulated lights changed drastically as the incident wavelength deviates from the designed one. Recently, metasurface [9–24], the two-dimensional planar meta-device composed of resonant sub-wavelength plasmonic or dielectric nanostructures, has emerged as an important candidate to reproduce computer-generated holograms [25] due to its advantages in manipulating amplitude, phase, and polarization of an electromagnetic wave at sub-wavelength scale. By merging two sets of independent plasmonic nanoantenna arrays in the same interface with low polarization crosstalk, researchers have proposed polarization-multiplexed metasurface holograms [14,16,17,23], in which local plasmoic resonance of individual nanoantenna can be selectively addressed according to the orthogonal linear [14,16,23] or helical polarization status [17,23]. Different from traditional polarization-multiplexed holograms, this introduces an alternative to exhibit the polarization-controlled dual images with high contrast over a broad frequency range. However, all demonstrated polarization-selective holograms consist of metal components, suffering from low diffraction efficiency and poor image quality due to the non-radiative ohmic loss and orthogonal polarizations coupling.

Free from Ohmic loss, dielectric metasurfaces [10–13,18] built up with nanostructures of high refractive index have been used in the design of optical devices due to

(a) E-mail: gydong@ucas.ac.cn
(b) E-mail: optsys@gmail.com
(c) E-mail: bike@bupt.edu.cn

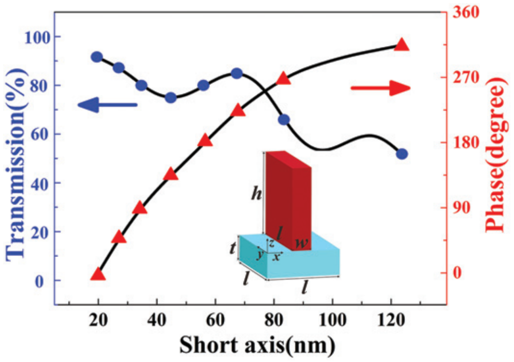

Fig. 1: (Color online) Transmission and phase modulation *vs.* the short-axis length of the Si-nanoblock at a unit period of 200 nm. The insert shows the constituent basic unit cell of the metasurface.

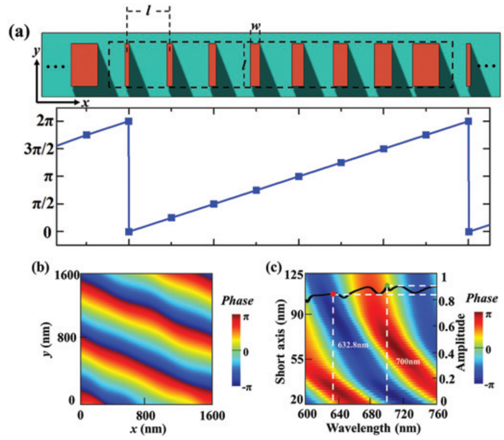

Fig. 2: (Color online) (a) The super cell of Si-nanoblocks for wave front shaping with same geometric parameters except for different short-axis sizes (20, 27, 35, 45, 56, 68, 83 and 125 nm). (b) Phase distribution of the transmission y-polarized light. (c) Phase modulation of the individual nanoblock *vs.* short-axis length from 20 to 125 nm and incident wavelength over the spectrum range of 600–760 nm. The insert black curve shows the simulated transmittance of the gradient metasurface with incident wavelength from 600 to 760 nm.

their easy-tuning electromagnetic scattering properties and higher transmission efficiencies with full range (0–2π) control. Silicon, the most commonly used material in semiconductor industry, enables dramatic enhancement in transmission efficiency, which makes it an ideal element for the design of a high efficiency metasurface. In this paper, we proposed a polarized-multiplexed broadband hologram based on a transmissive-type all-dielectric metasurface with high efficiency, high contrast and high image quality around the 600–760 nm visible range. Utilizing the polarization-dependent light-matter interaction effect, two set of holograms composed of Si-nanoblocks were encoded simultaneously on the same metasurface to reconstruct different images with the illumination of orthogonal linearly polarized light. Numerical simulation and experiment have proved the feasibility and adjustability of this polarization-multiplexed metasurface hologram.

Principle and design of polarized-multiplexed hologram. – The intensity of the polarized electric field along the long axis of a rectangle nanoblock is much stronger than that along the short axis in the process of light-object interaction [26,27]. In other words, if the dielectric nanoblocks satisfy the condition of the long axis oriented in the polarized direction of the field they can resonate, which can act as “switch on” or “switch off” with the change of the polarized status of incident light, providing an effective approach to realize a polarized-selectivity hologram. In this work, the Si-nanoblock, as shown in the insert of fig. 1, is employed as the basic element due to its low loss and low crosstalk between different polarization states. The constituent Si-nanoblocks with different widths along the short axis, the same length of 200 nm along the long axis and height of 320 nm were patterned on top of a 100 nm thick silica substrate with the unit period of 200 nm, center to center. Each Si-nanoblock behaves as a nanoantenna with its long axis always oriented to the polarization direction of the incident beam.

Under the illumination of the corresponding polarized light, some guided modes with dramatic phase modulations of transmitted light can be excited by varying the width of the nanoblock along the short axis. Finite Difference Time Domain (FDTD) Method was used to derive the structural parameters of the nanoblock for 0–2π phase modulation. The results of phase distribution and transmission amplitude are shown in fig. 1 as a function of the nanoblock width for the normal incident plane-wave at a wavelength of $\lambda = 632.8$ nm with polarization along the long axis. Considering the diffraction efficiency and fabrication compatibility, we select eight width stages (w = 20, 27, 35, 45, 56, 68, 83 and 125 nm) of a nanoblock to design a 8-level dielectric metasurface hologram with the 45° phase gradient interval. Although the same phase variation may cause non-uniform amplitude modulations, the average diffraction efficiencies of the selected eight nanoblocks are still high, which can be beneficial to high quality holographic images.

Figure 2(a) gives a super cell of the gradient metasurface composed of eight Si-nanoblocks with the gradual widths in a phase increment of $\pi/4$ to achieve 0–2π phase modulation. The periodic boundary conditions are used around the super cell to form an infinite plane structure with period of $T = 1600$ nm and phase gradient of $(\nabla\varphi)_x = 2\pi/\mathrm{T}$. Due to the tangential wave vector component $k_x = (\nabla\varphi)_x$, if the y-polarized light is normally incident onto the array plane, the angle of transmitted light can be calculated from the theoretical expression $\theta_t = \sin^{-1}(k_x/k_0) = 23.3°$, where k_0 is the wave vector of free space. Figure 2(b) shows the calculated phase distribution in the transmission space for the normal incident light at the wavelength of 632.8 nm. Obviously, the transmitted light is deflected by the whole

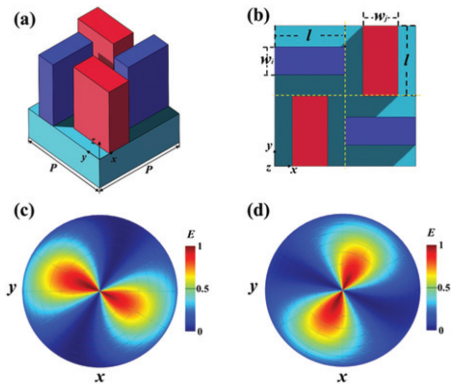

Fig. 3: (Color online) (a) One pixel of the polarized-multiplexed meta-hologram device with a size of 400×400 nm^2. (b) Top-view of the unit cell, with the inserts of long axis l, short axis w and yellow unit dividing dotted line. The simulated field intensity distribution of one pixel under the illumination of (c) x-polarized and (d) y-polarized light, respectively.

nanoblock-array metasurface with a slant angle of 23.19°, which agrees well with the theoretical result of 23.3°. For the Si-nanoblocks with a height of 100 nm, phase change of 2π only occurs around a fixed frequency with a narrow bandwidth based on the dipoles overlap due to the perfect match of electric and magnetic resonances [18]. Here, waveguide modes can be aroused in the Si-nanoblocks with the higher height of 320 nm to excite the phase shift of 2π with the broadband effect [28]. Figure 2(c) illustrates the phase pattern according to different short-axis lengths and wavelengths in this case, where 0–2π phase modulation can be achieved over a wide spectrum range of 600–760 nm. In addition, as the black curve shown in fig. 2(c), the transmittance of the whole metasurface composed of this kind of super cell with $h = 320$ nm was measured to illustrate the considerable diffraction efficiencies of 91.5% at 700 nm, 82.3% at 632.8 nm and more than 78% around the wide spectrum 600–760 nm.

Utilizing the polarization dependence of the light-matter interaction, two kinds of Si-nanoblocks with orthogonal long-axis directions were arranged to form a sub-wavelength unit which can powerfully echo with the corresponding polarized lights simultaneously. As shown in fig. 3(a), a pixel unit consists of four Si-nanoblocks with blue color to note one group responding to horizontal polarized (x-direction) light and red color to note another group responding to vertical polarized (y-direction) light. Figure 3(b) gives the top-view of the pixel unit with the nanoblocks arranged in a "swastika" shape, and two nanoblocks in the same group are arranged with a displacement vector of (l, l) symmetrically to enhance the contrast of holographic images and diffraction efficiency of the corresponding polarized component. For each polarization mode, arbitrary phase modulation can be achieved by varying the width w of the nanoblock along the short axis as mentioned in fig. 1. The simulated results in figs. 3(c) and (d) give the radiated far-field intensities of a single pixel unit of 400×400 nm^2 induced by x-polarized and y-polarized normally incident lights, respectively. As expected, linear polarized light strongly interacts with the nanoblocks of the parallel long axis to obtain a distinct diffraction pattern, and the diffraction patterns excited by the orthogonal x- and y-polarized lights keep a low cross-talk, which demonstrate that the designed pixel unit can intensely respond to the orthogonal polarized lights, respectively.

Numerical simulation and analysis. – The specific pixel unit characters of independent orthogonal polarizations make it possible to realize the reconstructions of different target images through a dual-channel phase-only hologram composed of properly designed "swastika" units. Using the classical Gerchberg-Saxton (GS) algorithm [29], the two required phase profiles of target images "O" and "K" are retrieved and then encoded into various short-axis sizes of Si nanoblocks in designed "swastika" pixel units. As illustrated in the fig. 4(a), an ultrathin metasurface composed of 2D array of pixel units imprinted phases for orthogonal polarized components simultaneously serves as a synthetic polarization-selectivity hologram, which reconstructs holographic images either "O" or "K" under the illuminations of horizontal or vertical polarized light, respectively. In order to reduce the need for computer simulation memory and reproduce clear images at the lowest possible pixel units, the metasurface composed of 40×40 pixel units (*i.e.*, 80×80 nanoblocks) is employed as the polarized-selectivity hologram in this simulation. The numerical simulation is equivalent to placing a screen at the far enough distance of 1 m away from the metasurface to perform Fourier transform, and the extracted target images are given by

$$|P_i(u,v)|^2 = |FT\{P_i(x,y)\}|^2, \tag{1}$$

where $P_i(x,y)$ is the distribution of phase information. Figures 4(b) and (c) show the two reconstructed holographic images "O" and "K" in the cases of 632.8 nm x-polarized and y-polarized illuminations, respectively, which confirm the polarization-multiplexed function of the designed metasurface hologram. Under the illumination of 45° linear-polarized light beam, the two images overlap each other due to the orthogonal decomposition of incident light, as shown in fig. 4(d). Their intensities are just simple superposition because of the non-interactive effect between the two orthogonal polarizations. The same phenomenon can be achieved by the circularly polarized lights with a phase difference of $\pm\pi/2$ between the two orthogonal polarization components. In addition, the spotted noises were found in the reconstruction images due to the phase discreteness, which can be dramatic improved by increasing the phase level. Although the transmission amplitude of each unit cell is not completely uniform, the high contrasts of those simulated holographic images provide a clear authentication of target images which can be viewed by direct visual inspection. Furthermore, the designed

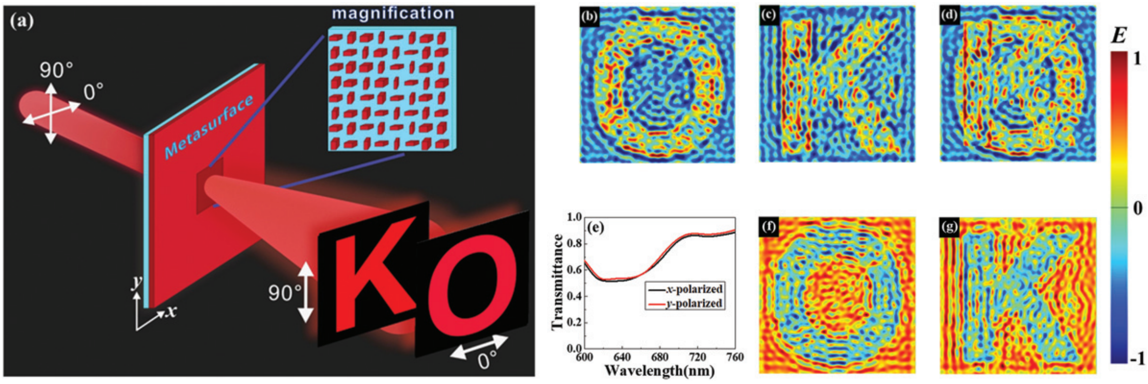

Fig. 4: (Color online) (a) Illustration of our designed metasurface hologram under two orthogonal polarized illuminations. The phase distribution of the two images "O" and "K" were encoded on the same metasurface and can be reconstructed by the linearly polarized light along the x- or y-direction, respectively. Reconstructed holographic images for (b) x-polarized, (c) y-polarized and (d) 45°-polarizated under 632.8 nm illumination. (e) The transmission efficiency of two diffracted emissions over the bandwidth from 600 nm to 760 nm for two orthogonal polarized positions. Reconstructed holographic images for (f) x-polarized and (g) y-polarized under the 700 nm illumination.

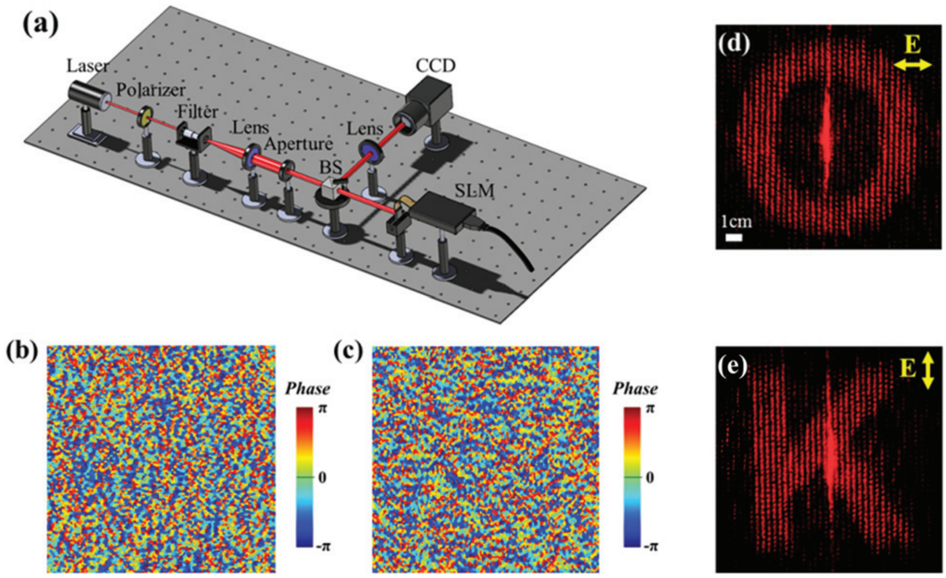

Fig. 5: (Color online) (a) Illustration of the experimental set-up of the polarized-selective meta-hologram. The simulated phase patterns of the required images "O" and "K" using FDTD with (b) x-polarized and (c) y-polarized incident light. (d), (e) The corresponding experimentally holographic images by illuminating the phase information in (b) and (c) recorded by SML with the (d) x-polarized and (e) y-polarized incident light, respectively.

meta-hologram maintains a high transmission efficiency spanning a wide bandwidth of 160 nm, especially with an efficiency over 80% at $\lambda > 700$ nm, as shown in fig. 4(e). The extracted holographic images in figs. 4(f) and (g) under the illumination at 700 nm also give a strong evidence for the broadband characteristics of designed metasurface.

Experimental results. – As a proof-of-concept demonstration, fig. 5(a) shows the experimental set-up to characterize the performance of the designed meta-hologram. The spatial light modulator (SLM) [30] can imitate a standard hologram to yield a reprogrammable optical wavefront under computer control, so the meta-hologram was replaced by SLM in our experiment for convenience. Different from traditional computer-generated holograms (CGH) with holographic fringe pattern obtained by simple sampling, calculation and coding, here the holographic profile, that is, the phase-only profile imprinted on the metasurface, was calculated by using the FDTD method. Figures 5(b) and (c) show the calculated phase patterns. HOLOEYE PLUTO reflex phase-only SLM was used in our experiment to act as the meta-holograms for the x- and y-polarized phase patterns illustrated in figs. 5(b) and (c). A laser beam with 632.8 nm linearly polarization generated by the He-Ne laser source and polarizer is incident on the SLM with a beam radius of ∼5 mm to ensure the phase information area could be illuminated entirely. The reflected holographic images were captured by a charge coupled device (Coolsnap EZ CCD). It is clear that the reconstructed holographic images of "O" and "K" shown in figs. 5(d) and (e) have a high fidelity and less distortion, which agree well with the previous theoretical and simulation results. Due to the on-axis set-up of SLM, the zero-order diffraction pattern appeared at the center of the reconstructed holographic images, but they do not affect the contrast and quality of images, which can be improved by optimizing the multiple-level phase and sub-wavelength pixel size of the meta-hologram.

Discussion. – The polarization-multiplexed metasurface hologram not only provides a new method to integrate multiple hologram patterns into one hologram but also brings an immediate impact on security and authentication. The various complex freedom degree of an optical waveform, such as wavelength, polarization and respond bandwidth, can be employed as security key to make information more difficult to be attacked. As in our design, each type of polarized component independently manipulates one set of the phase profile, so only the corresponding polarized light can reconstruct the according image. Additionally, the operating wavelength can be selected in a wide responsive band from 600 nm to 760 nm which not only increases the flexibility of our hologram, but also further guarantees the security of the target information. For example, if the incident light is within the designed wavelength ranges, the positive holographic image can be still extracted. In contrast, if the wavelength deviates from the responded bandwidth, it could result in negative authentication. In short, all the properties of the designed metasurface hologram will possess a unique advantage in the hologram-encryption system.

Amorphous silicon (a-Si) has been widely used in the metasurface hologram due to its high transmission, low loss and easiness in being deposited on any kind of substrate. However, the operating wavelength of a-Si is often limited to $\lambda > 600\,\text{nm}$ for its high absorption below 600 nm [19]. In order to compensate this shortage, the original materials of nanoblocks of the meta-hologram can be replaced by other dielectric materials, such as crystalline silicon (c-Si) or titanium dioxide (TiO_2) to extend the response bandwidth to a visible spectrum range.

Conclusion. – In conclusion, we have implemented a new kind of polarized-selectivity metasurface hologram capable of reconstructing different holographic images with high efficiency and high contrast over a broadband spectrum range of 600-760 nm. Si-nanoblocks with fixed long-axis size along two orthogonal directions and diverse short-axis sizes were employed to imprint two sets of phase profiles of different target images on a metasurface. Normal incident lights of linear or circular polarization falling onto the metasurface can reconstruct different holographic images. Simulations and experimental results agree well with the theoretical analyses. The polarization-multiplexed hologram provides a new approach for the designs of future optical functional devices in optical storage, encryption, multistage optical switching and optical interconnection network.

* * *

This work was supported by the National Natural Science Foundation of China under Grant Nos. 11574311, 61575197, 61774020, 61775121, Shandong Provincial Natural Science Foundation of China under Grant No. ZR2016FM03.

REFERENCES

[1] Kawano K., Ishii T., Minabe J., Niitsu T., Nishikata Y. and Baba K., *Opt. Lett.*, **24** (1999) 1269.
[2] Tan X., Matoba O., Okada-Shudo Y., Ide M., Shimura T. and Kuroda K., *Appl. Opt.*, **40** (2001) 2310.
[3] Krishnamoorthy A. V., Xu F., Ford J. E. and Fainman Y., *Appl. Opt.*, **36** (1997) 997.
[4] Johnson K. M., Surette M. R. and Shamir J., *Appl. Opt.*, **27** (1988) 1727.
[5] Ford J. E., Xu F., Urquhart K. and Fainman Y., *Opt. Lett.*, **18** (1993) 456.
[6] Xu F., Ford J. E. and Fainman Y., *Appl. Opt.*, **34** (1995) 256.
[7] Zeitner U. D., Schnabel B., Kley E.-B. and Wyrowski F., *Appl. Opt.*, **38** (1999) 2177.
[8] Yu W. J., Konishi T., Hamamoto T., Toyota H., Yotsuya T. and Ichioka Y., *Appl. Opt.*, **41** (2002) 96.
[9] Yu N. F., Genevet P., Kats M. A., Aieta F., Tetienne J. P., Capasso F. and Gaburro Z., *Science*, **334** (2011) 333.
[10] Yang Y., Wang W., Moitra P., Kravchenko II, Briggs D. P. and Valentine J., *Nano Lett.*, **14** (2014) 1394.
[11] Shalaev M. I., Sun J., Tsukernik A., Pandey A., Nikolskiy K. and Litchinitser N. M., *Nano Lett.*, **15** (2015) 6261.
[12] Wang L., Kruk S., Tang H., Li T., Kravchenko I., Neshev D. N. and Kivshar Y. S., *Optica*, **3** (2016) 1504.
[13] Wang B., Dong F., Li Q. T., Yang D., Sun C., Chen J., Song Z., Xu L., Chu W., Xiao Y. F., Gong Q. and Li Y., *Nano Lett.*, **16** (2016) 5235.
[14] Montelongo Y., Tenorio-Pearl J. O., Milne W. I. and Wilkinson T. D., *Nano Lett.*, **14** (2014) 294.
[15] Zheng G., Muhlenbernd H., Kenney M., Li G., Zentgraf T. and Zhang S., *Nat. Nanotechnol.*, **10** (2015) 308.
[16] Chen W. T., Yang K. Y., Wang C. M., Huang Y. W., Sun G., Chiang I. D., Liao C. Y., Hsu W. L., Lin H. T., Sun S., Zhou L., Liu A. Q. and Tsai D. P., *Nano Lett.*, **14** (2014) 225.
[17] Wen D., Yue F., Li G., Zheng G., Chan K., Chen S., Chen M., Li K. F., Wong P. W., Cheah K. W., Pun

E. Y., Zhang S. and Chen X., *Nat. Commun.*, **6** (2015) 8241.
[18] Yu Y. F., Zhu A. Y., Paniagua-Domínguez R., Fu Y. H., Luk'yanchuk B. and Kuznetsov A. I., *Laser Photon. Rev.*, **9** (2015) 412.
[19] Yoon G., Lee D., Nam K. T. and Rho J., *ACS Photon.*, **5** (2017) 1643.
[20] Deng Z. L., Zhang S. and Wang G. P., *Nanoscale*, **8** (2016) 1588.
[21] Deng Z. L., Wang G. P. and Zhang S., *Opt. Express*, **24** (2016) 23118.
[22] Deng Z. L. and Li G. X., *Mater. Today Phys.*, **3** (2017) 16.
[23] Deng Z. L., Deng J. H., Zhuang X. *et al.*, *Nano Lett.*, **18** (2018) 2885.
[24] Deng Z. L., Gao Y. Y., Li X. P. and Wang G. P., *Photon. Res.*, **6** (2018) 443.
[25] Slinger C., Cameron C. and Stanley M., *Computer*, **38** (2005) 46.
[26] Khorasaninejad M., Zhu W. and Crozier K. B., *Optica*, **2** (2015) 376.
[27] Khorasaninejad M. and Crozier K. B., *Nat. Commun.*, **5** (2014) 5386.
[28] Li Q. T., Dong F., Wang B., Gan F., Chen J., Song Z., Xu L., Chu W., Xiao Y. F., Gong Q. and Li Y., *Opt. Express*, **24** (2016) 16309.
[29] Gerchberg R. W. and Saxton W. O., *Optik*, **35** (1971) 237.
[30] Weiner A. M., *Rev. Sci. Instrum.*, **71** (2000) 1929.